science.sciencemag.org/content/366/6468/1008/suppl/DC1

Supplementary Materials for

A cortical-brainstem circuit predicts and governs compulsive alcohol drinking

Cody A. Siciliano*, Habiba Noamany, Chia-Jung Chang, Alex R. Brown, Xinhong Chen, Daniel Leible, Jennifer J. Lee, Joyce Wang, Amanda N. Vernon, Caitlin M. Vander Weele, Eyal Y. Kimchi, Myriam Heiman, Kay M. Tye*

*Corresponding author. Email: tye@salk.edu (K.M.T.); cody.siciliano@vanderbilt.edu (C.A.S.)

Published 22 November 2019, *Science* **366**, 1008 (2019)
DOI: 10.1126/science.aay1186

This PDF file includes:

Materials and Methods

Animals and Stereotaxic Surgeries: Male C57BL/6J mice were used for all experiments (Jackson Laboratory). Animals arrived at 8 weeks of age, and were allowed to acclimate to the facility for at least one week before any testing or surgery was performed. Animals were housed in a reverse 12-hour light-dark cycle room and maintained on light food restriction (~3g/animal/day, maintained at 25-30 grams per animal) and *ad libitum* water. All surgeries were conducted under aseptic conditions using a digital small animal stereotaxic instrument (David Kopf Instruments, Tujunga, CA, USA). Animals were anesthetized using isoflurane (5% for induction and 1-2% for maintenance). Injections were performed using a beveled 33-gauge microinjection needle. A 10 mL microsyringe (nanofil; WPI, Sarasota, FL, USA) was used to deliver virus at a rate of 0.1 mL per min using a microsyringe pump (UMP3; WPI) and controller (Micro4; WPI).

All experiments involving the use of animals were in accordance with NIH guidelines and approved by the MIT Institutional Animal Care and Use Committee. For all experiments involving viral injections and/or implants, animals containing mistargeted injection(s) were excluded after histological verification.

Surgery for *in vivo* calcium imaging: Subjects were prepared for *in vivo* epifluorescent calcium imaging as described previously(*24*). In brief, to achieve projection-specific imaging, a virus encoding Cre-dependent GCaMP6m (AAV_5-CAG-FLEX-GCaMP6m) was injected into the mPFC (AP: +1.8, ML: +0.3, DV: −2.75 and −2.4 (300 nl at each DV location)) and retrogradely-travelling CAV2-Cre(*31*) (Institut de Génétique Moléculaire de Montpellier, France) was injected into the dPAG (AP: −4.2, ML: +0.5, DV: −2.4 (300 nl)). After viral infusions, the mPFC craniotomy was enlarged to >1 mm in diameter and dura mater was removed with a bent 30 gauge beveled needle, but no tissue was aspirated. A 1 mm diameter, ~4 mm length gradient index lens (GRIN lens; GLP-1040, Inscopix) was held by vacuum on the tip of a blunted needle with plastic tubing attached for stability and was lowered stereotaxically through the craniotomy under constant saline perfusion to minimize tissue/blood desiccation. Lenses were implanted slightly posterior and lateral of the needle track for virus infusions to avoid tissue damage in the imaging plane, and were lowered to locations in the ventral PL/dorsal lL subregion of the mPFC (AP: −1.77, ML: −0.4, DV: −2.45, mm from bregma). Lens implants were secured to the skull with a thin layer of adhesive cement (C&B Metabond; Parkell), followed by black cranioplastic cement (Ortho-Jet; Lang) containing gentamicin antibiotic. Lenses were covered with the top of an Eppendorf tube and cemented in place with cranioplastic cement for protection during the virus incubation period (6-8 weeks). The implant was allowed to completely dry before closure of the incision with nylon sutures.

Following viral incubation, mice were again anaesthetized with isoflurane, stereotaxically secured, and baseplates (Inscopix) were cemented around the lens to support the connection of the miniaturized microscope for *in vivo*, freely moving imaging. During this procedure, the protective Eppendorf cap and supporting cranioplastic cement were removed using a hand drill. The exposed top of the GRIN lens was scrubbed clean with a cotton-tipped applicator soaked with 15% isopropyl

alcohol diluted in ddH2O. Next, a miniaturized microscope (single channel epifluorescence, 475-nm blue LED, Inscopix) with the baseplate attached was stereotaxically positioned over the implanted GRIN lens and adjusted in the DV axis in order to focus on visible landmarks (that is, GCaMP6m-expressing neurons and blood vessels). After the focal plane was identified, the microscope/baseplate was raised by ~30 μm, to account for cement shrinkage, and was subsequently cemented in place with dental cement (Stoelting). The microscope was then detached from the baseplates, a final layer of black cranioplastic cement (Ortho-Jet; Lang) was applied to prevent light leak, and the implant was covered with a protective plate (Inscopix) until imaging.

Binge-Induced Compulsion Task (BICT):

Apparatus (Skinner box): All conditioning experiments were performed in a Skinner box (Med Associates) intended for use with rats. A rat reward port was used to allow room for head entries when tethered to a head-mounted miniature microscope (Inscopix), and the box was divided in half by a plastic divider to limit exploratory behavior. Infrared beam-breaks for head-entry detection were removed from the reward port and replaced with an electrical lickometer to avoid any interference with imaging equipment. A blunted 18-gauge needle connected to a syringe pump was inserted through the back of the reward port so that fluid could be delivered to the front of the port. Fluid formed a small bubble at the tip of the syringe, which was wired such that contact with the needle or fluid were recorded by the lickometer. All sessions were run in the dark, and mice were monitored with infrared cameras positioned above the chamber. Two speakers, one for white noise and one for tone presentation (see below) were located on the wall opposite the reward port. The camera was used to monitor the animals' behavior throughout the task by an experimenter to ensure that any potential tangling of the microscope wire did not impede the animals' movement.

Trial structure: Throughout all phases of the task, the trial structure remained consistent. All conditioning sessions took place in a Skinner box, described above. The start of the session was signaled by the onset of white noise (60dB) which remained on throughout the session. The first trial began 60 seconds after the onset of the session. Intertrial intervals were variable with an average of 60 seconds. The behavioral apparatus was interfaced with the miniature microscope such that the microscope could be controlled, and behavioral events could be timestamped into the recording. Each trial began with triggering the miniature microscope to turn on the LED, and frames were collected at 20Hz throughout the trial (LED remained off during ITIs to minimize phototoxicity). Ten seconds after turning on the microscope, an auditory cue (2 or 8kHz) was presented for 5 seconds. On CS+ trials, two seconds after the offset of the tone (seven seconds after onset) fluid was delivered to the reward port (10μL delivered over one second). On CS- trials, no fluid was delivered. Forty seconds after the start of the trial the microscope LED was turned off, and the intertrial interval began. On subsequent trials, if no lickometer contacts were detected since the last fluid delivery, cues would still be presented but no additional fluid would be delivered until licks were detected to avoid fluid buildup in the reward port. Each session lasted one hour. At the end of every session, any remaining fluid in the port was measured with a pipette to determine each animal's total consumption (number of deliveries multiplied by 10μL minus any

remaining fluid). Mice were weighed and daily food was given in the home cage immediately following each session. This trial structure was used throughout all of the phases of the BICT, described below, unless otherwise noted.

Training: Training began at least 8 weeks after surgery to allow time for virus expression. Prior to the first session, animals were exposed to 10% sucrose solution (diluted in water) in the home cage (~0.5 mL per animal left in the cage overnight). Animals were randomly assigned to have either a 2 or 8 kHz tone (counterbalanced between animals) for CS+ trials, and the other for CS- trials. For each animal, the tones used for CS+ and CS- were kept consistent throughout the entire task regardless of the unconditioned stimulus. Tones intensities were 75dB, measured at the speaker located on the opposite wall from the reward port. A multi-step protocol was used for training, with acquisition criteria at each step. During training, the unconditioned stimulus was 10% sucrose diluted in water (w/v). For the initial training phase, only CS+ trials were presented. For the first session, animals were not tethered, and allowed to explore the chamber and reward port until 10 rewards were collected, at which point the session was paused, animals were tethered to the miniature microscope, and allowed to complete the rest of the session. Mice were tethered for all conditioning sessions from this point forward. Once animals consumed sucrose on >90% of trials in a session, they were moved on to the discrimination phase. During discrimination, animals were presented with CS+ (70% of trials) and CS- (30% of trials) trials in pseudorandom order. Lick rate was assessed across all of the trials for a given session and normalized to a 10 second pre-tone baseline period. Animals were considered to have acquired discrimination once lick rate passed a 4 z-score threshold within 3 seconds of sucrose delivery on CS+ trials, but did not cross this threshold on CS- trials, and these criteria were met for two consecutive sessions. Once these criteria were met, all animals were given one additional session with identical conditions, except that CS+ tones predicted the delivery of a 10% sucrose + 15% alcohol solution.

Pre-Binge: On the day following completing all acquisition criteria, animals began the Pre-Binge conditioning epoch. Conditions were identical to the discrimination phase of training (70% CS+ trials, 30% CS- trials), except that the unconditioned stimulus was 15% alcohol (v/v) in water without any sucrose. Alcohol was available for three consecutive sessions (Alcohol only sessions). In sessions four and five, alcohol concentration remained at 15%, but the solution was adulterated with quinine (250µM for session four, 500µM for session five) (Alcohol+quinine sessions).

Binge Drinking: On the day following the completion of the Pre-Binge epoch, animals began a two-bottle choice procedure, used to model binge drinking. This paradigm was based on the “drinking in the dark” procedure(*22*, *32–34*), with several modifications. The most notable modification was that water was always concurrently available with alcohol. At 0930 hours, 1.5 hours after the beginning of the dark cycle, each animal was separated from their home cage, individually placed into a clean home cage, and allowed to acclimate for 30 minutes. At 1000 hours, 2 hours into the dark cycle, two bottles containing water or 15% alcohol (v/v) were placed on the wire cage top with the spout extending into the cage (bottle location was switched each day to avoid effects

driven by side preference). Bottles were weighed immediately before and after the session, and consumption volume was inferred from the difference in weight. For the first four days, mice were given two hours of access (bottles removed at 1200 hours), followed by four hours of access on the fifth day (bottles weighed at 1200 hours, and returned for another 2 hours before being weighed again). The following two days, mice were forced to remain abstinent, and no procedure was performed. This one-week cycle (two-hour access for days 1-4, four-hour access on day 5, abstinence on days 6-7) was repeated for a second time before beginning the Post-Binge epoch.

Post-Binge: The post-Binge epoch began the day following the final forced abstinence day of the Binge Drinking epoch. Testing was performed in the same context as Pre-Binge sessions, and parameters were identical. After three sessions of alcohol availability, quinine was again introduced to the solution. In the Post-Binge epoch, four quinine sessions were given instead of two. Quinine concentrations were again presented in ascending order across sessions (250, 500, 750, 1000 µM mixed in 15% alcohol).

Behavioral analysis*:* Alcohol intake during the Pre-Binge and Post-Binge sessions was expressed as a percent of the total that could have been theoretically obtained (number of CS+ trials multiplied by 10µL). To determine each animal's phenotype, alcohol consumption during the Post-Binge epoch was averaged across the three Alcohol only session and the four Alcohol+quinine sessions, and these averages were then plotted as normalized distributions across animals for each of the two measures [animals' average intake/average of the group]. Animals with values above the average of the Alcohol and Alcohol+quinine distributions were deemed 'Compulsive'. Those with values above the average of the Alcohol only distribution, but below the average of the Alcohol+quinine distribution were deemed 'High Drinkers'. Animals with values below the average for both distributions were deemed 'Low Drinkers'. Distributions calculated from both the Pre-Binge and Post-Binge data are presented, but only the Post-Binge data were used to assign phenotypes. The phenotypes assigned from the Post-Binge data was used for all analyses. Values from the Alcohol only and Alcohol+quinine distributions were summed to create an 'alcohol use index' for each animal. The alcohol use index was used to summarize each animals' alcohol use disorder-like behaviors.

To assess the ability of quinine to inhibit alcohol consumption for each phenotype, intake during quinine sessions were plotted as a percent of the Alcohol only sessions and fitted with non-linear dose response curves (Graphpad Prism V6: log[inhibitor] vs. normalized response, variable slope) to interpolate the IC_{50} of quinine (the concentration of quinine required to produce a half-maximal effect of quinine on alcohol consumption).

For analysis of Binge Drinking data, consumption was expressed as grams of alcohol intake per kilogram of animal weight per two hours of access (g/kg/2 hours). Animal weight was recorded immediately following each session. Alcohol preference was calculated by dividing the total volume consumed from the alcohol bottle across all sessions by the total fluid volume consumed across all sessions [alcohol volume/(alcohol + water volume)].

Calcium imaging analysis:

Image processing and signal extraction: Image processing was accomplished using Mosaic software (v.1.1.2., Inscopix). Raw videos were pre-processed by applying 4x spatial downsampling to reduce file size and processing time, and isolated dropped frames were corrected. No temporal downsampling was applied. For each animal, all of the 40 second trials for each session were concatenated to generate a single video. Lateral movement was corrected for by using a portion of a single reference frame as previously described(*35*, *36*). Images were cropped to remove post-registration borders and sections in which cells were not observed. Videos were then exported as TIF stacks for analysis.

After motion correction and cropping, we used a modified version of a constrained non-negative matrix factorization algorithm optimized for micro-endoscopic imaging (CNMF-E)(*37*) to extract fluorescence traces from neurons. Neurons were defined by manually selecting seed pixels from peak-to-noise (PNR) graphs of the field of view (FOV)(*38*). Considering calcium fluctuations can exhibit negative transients, associated with a pause in firing(*39*), we did not constrain temporal components to >=0, as previously described(*24*). All neurons were visually inspected following CNMF-E, and those that displayed non-neuronal morphology were removed.

Calcium activity quantification: Stimulus-evoked activity was assessed by aligning calcium activity traces around cue onset or onset of licking for alcohol. The behavioral apparatus was interfaced with the miniature microscope via BNC cables and the onset of cues and licks were associated with a frame of the video using transistor-transistor logic (TTL). For each neuron across all trials, activity traces from eight seconds before and eight seconds after each event were extracted. For responses to alcohol consumption, traces were aligned to the first lickometer contact after the delivery of alcohol on CS+ trials. Each extracted trace was then normalized to a pre-stimulus baseline window using a z-score transformation. For traces aligned to the first lick for alcohol, a three second baseline window from 8 to 5 seconds prior to the lick was used. For traces aligned around cue onset, a three second baseline window of 5 to 2 seconds prior to cue onset was used. Z-scored traces were then averaged across trials to create one trace per neuron for each stimulus type. The values from the time of stimulus until one second later were averaged, and this value was used to determine the response profile of each cell. Cells with an average of greater than 3 z-scores during the one second post-stimulus window were classified as having an excitatory response, while those with less than -3 z-scores were classified as having an inhibitory response. Given that number of alcohol trials completed varied across animals, trial number was matched *post-hoc* to ensure that effects were not driven by differential sample size between the groups. Only the first *n* trials completed for each animal were analyzed, where *n* was equal to the lowest number of trials completed across animals for that session. Further, a minimum of eight trials completed were required to be included in the analysis; one animal (from the Low Drinker group) was excluded from calcium imaging analysis in Figure 2 based on this criterion. All data displayed in Figure 2 were collected during the first session of the Pre-Binge epoch.

In Figure 2H, to display the population activity during alcohol consumption, all neurons that showed significant responses (both excitatory and inhibitory) to alcohol

(using the criteria explained above) were averaged together for each animal. The resulting activity traces were then averaged together by group (n=50 cells for Low Drinkers, n=49 cells for High Drinkers, n=35 cells for Compulsive animals). To quantify the magnitude of the response, area under the curve for each animal's averaged population trace was calculated. The area was calculated from two seconds prior and two seconds after the lick. Peaks above zero resulted in positive area while those below zero resulted in negative area, and the area of all peaks within the four second window were summed to create a net area value for each animal.

To determine the balance of excitatory and inhibitory activity during alcohol consumption, the percentage of cells that showed inhibitory responses during alcohol consumption was subtracted from the percentage of cells that showed excitatory responses for each animal. This excitation/inhibition value was determined from the neural activity during the first day of Pre-Binge, and then separately correlated with the alcohol use index calculated from the Pre-Binge, Binge, and Post-Binge data for each animal.

Hierarchical clustering: For agglomerative clustering, we first averaged responses of individual neurons aligned to the first lick after alcohol delivery across trials (expressed in z-scores), such that each row in the heatmap corresponds to one neuron. We then clamped the original response profiles with the lower and upper bound of z-score in the heatmap. Agglomerative hierarchical clustering was applied using Ward's Euclidean linkage. Pairs of neurons that were in close proximity were linked. As they were paired into binary clusters, the newly formed clusters were grouped into larger clusters until a hierarchical tree was formed. A threshold at 0.245 × max(linkage) was set to prune branches off the bottom of the hierarchical tree, and assign all the neurons below each cut to a single cluster. After clusters were constructed, data was separated to generate their individual heat maps using their original average response profiles. For visualization purpose, clusters and neurons within each cluster were sorted in an ascending order on the basis of their average response to the alcohol. Different bars on the right side of the heat maps correspond to different clusters. The same color denotes that they belong to the same cluster from the dendrogram. All neurons from each cluster were averaged and smoothed to create a peri-stimulus time histogram of activity during alcohol consumption for each cluster.

Machine Learning (support vector machine classifier): A machine-learning algorithm(*40*) was used to determine whether ensemble dynamics in mPFC-dPAG neurons during the consumption of alcohol in a given trial could encode the animal's decision to consume/collect alcohol on the subsequent CS+ trial. We analyzed calcium activity from five Pre-Binge sessions (three Alcohol only sessions, two Alcohol+quinine sessions), and a matched set of five Post-Binge sessions.

Calcium activity for each cell on each trial was aligned to the first lick after alcohol delivery. Data from 8 seconds before to 8 seconds after the lick was extracted. We reduced the dimensionality of ensemble activity within each session using principal components analysis (PCA), to extract sets of features for each trial. Features were then concatenated across all animals and sessions.

A subset of data from the first day was used to train a support vector machine (SVM) classifier to predict subsequent behavioral responses on the following CS+ trial (collection or no collection). Five-fold cross-validation was used to optimize SVM hyperparameters. After optimization, the trained decoder was applied to test data, including held-out data from the first session as well as from all subsequent sessions. Because collection trials were more common than no collection trials, a subset of collection trials were sampled to match the number of no collection trials to avoid bias in training, yielding an empiric chance accuracy rate of 50%. The decoding accuracy across mice for a given session was calculated as the percentage of trial predictions that corresponded with the subsequent behavior (collection or no collection).

Blood alcohol concentrations: Blood alcohol concentration was assessed to determine if inferred volumes of alcohol consumption were a reliable proxy measures of alcohol consumption. During conditioning sessions, alcohol intake was inferred from the volume of alcohol delivered across trials, and during Binge Drinking sessions intake was inferred from changes in the weight of the bottles (see Binge-Induced Compulsion Task section, above). Each animal that performed the BICT was bled once after a session. To avoid excessive stress, no animal was bled more than once, and the point in the task that the animal was bled was randomly assigned. Immediately following completion of the assigned session, animals were restrained, the submandibular vein was punctured with a lancet (5.5mm, Goldenrod), and blood was collected with a heparinized capillary tube (Kimble). Blood was transferred to an Eppendorf tube, and centrifuged to separate serum. Blood alcohol content was then assessed using a standard commercially available assay (Pointe Scientific).

Binge-Induced Compulsion Task re-test (shock punishment): ~70 days after the completion of the Binge-Induced Compulsion Task, a subset of animals were retested to determine 1) if the observed phenotypes were reproducible across time and 2) if the compulsive phenotype was affected by modality of the punishment. Animals were moved to different operant chambers so that testing could be performed in a distinct context. Animals were first given one day of conditioning where 15% alcohol mixed with 10% sucrose was available, to reinstate drinking behavior. From that point forward, methods were identical to the previous testing, with the exception that instead of increasing concentrations of quinine, shock was instead used to punish alcohol drinking. On shock days, shock was delivered one second after initial contact on the alcohol lickometer. Shock amplitude was presented in ascending order across days (50, 100, 200, 300μA).

Surgery for optogenetic experiments: For the photoinhibition experiments, 300 nl of a viral vector carrying the gene for a fusion protein comprised of enhanced halorhodopsin and enhanced yellow fluorescent protein under the calmodulin kinase IIα promoter (AAV_5-CaMKIIα-eNpHR3.0-eYFP) was bilaterally injected into the mPFC. Two optic fibers were implanted bilaterally over the dPAG and secured with a layer of adhesive cement followed by dental cement. For eYFP control animals, surgery was identical but AAV_5-CaMKIIα-eYFP was injected instead.

For the photoexcitation experiments, the double-inverted open reading frame (DIO) Cre-dependent expression system was used to excite the cell bodies of mPFC cells projecting to the dPAG. AAV_5-DIO-ChR2-eYFP was bilaterally injected into the mPFC (300 nl). CAV2-Cre was injected into the dPAG (250 nl), and two optic fibers implanted over the mPFC. For eYFP control animals, surgery was identical but AAV_5-DIO-eYFP was injected instead.

Real-time place preference/avoidance: A real-time place preference/avoidance assay as used to determine if manipulation of neural activity was preferred or avoided(*41*, *42*). Mice were restrained and fiber optic patch cables were attached to the implanted ferrules before being placed in a plexiglass arena (24 in (l) × 24 in (w) × 20 in (h)) and allowed to move freely between two compartments for 45 minutes. Entry into one side of the chamber trigged a laser on period, which lasted as long as the animal remained on that side (5mW of 589nm light delivered continuously for photoinhibition experiments; 10mW of 473nm light delivered in 5ms pulses at 20Hz for photoexcitation experiments). Mice were tested on two consecutive days, and on the second day the stimulation side and no stimulation side were reversed (order of which side was on/off first was counterbalanced across animals). A video camera positioned directly above the arena tracked and recorded movement using EthoVision XT (Noldus). All data presented are tracked from the 'center' of the subject, and time spent in each zone was averaged across the two testing sessions.

Intracranial self-stimulation: Intracranial self-stimulation was used to determine if manipulations of neural activity were capable of maintaining an operant response(*43*, *44*). Intracranial self-stimulation was performed in a standard Skinner box (Med Associates). Each box was equipped with two nose-poke ports (active and inactive, counter balanced across animals). Responding in the active poke was reinforced on a fixed-ratio 1 schedule, and resulted in light delivery through the patch cable (5mW of 589nm light delivered for 5 seconds) as well as presentation of a tone (2 or 8 kHz, counterbalanced between animals, for 5 seconds) and illumination of a cue light located above the lever. The inactive poke resulted in presentation of a distinct tone (2 or 8 kHz, counterbalanced between animals) and an identical light cue located above the inactive poke, but did not activate the laser. During the first session, both nose-pokes were baited with $1/8^{th}$ of a Froot Loop to encourage exploration of the nose-pokes. Nose-pokes were only baited on the first session. Animals were run for a total of 5 sessions, and each session was one hour long.

Elevated Plus Maze: An elevated plus maze assay was used to assess anxiety-related behavior(*45*). The elevated plus maze consisted of two closed arms (30 x 5 x 30 cm) and two open arms (30 x 5 cm) at 90° from each other, and a central platform (5 x 5 cm), all made of grey plastic. Mice were placed in the maze and allowed to explore for 10 minutes. The first minute was excluded as it was considered time for the animal to habituate to being placed in the EPM. A laser was turned on (either constant 589nm yellow light for the halorhodopsin experiments or 479nm blue light at 20Hz for ChR2 experiments) four minutes into the session for 3-minute ON epoch. The order in which

mice performed the task was counterbalanced across groups. The time spent in the center and open and closed arms was hand-scored by a blinded experimenter.

Light-dark box assay: A light-dark box assay was also used to assess anxiety-related behavior(*46*, *47*). Mice were restrained and attached to fiber optic patch cables before being placed in a clean home cage next to the behavioral apparatus for three minutes. They were then placed into a plexiglass arena (30 in (l) × 15 in (w) × 25 in (h)) divided into two compartments with a small opening between the sides. One side was brightly lit (350-400 lumens) and the other dimly lit (5-15 lumens). Mice were always placed into the light side of the arena, near the side farthest from the entrance to the light side, and laser light illumination began immediately (589nm, constant, 5mW measured at the tip of the patch cable). The session consisted of 3 epochs (laser on, laser off, laser on), each five minutes long, for a total of 15 minutes. Movement was tracked by an overhead video camera positioned above the arena, and latency to make the first cross into the dark side of the chamber as well as time spent in each compartment was calculated (EthoVision XT (Noldus)).

Tail flick assay: A tail flick assay was used to determine responses to nociceptive stimuli(*48*). Mice were placed in a restrainer with their tail extending from the end. Each animal performed two sets (one laser on, one laser off) consisting of two trials. Latencies from the two trials of each set were averaged to create one value per animal for each of the two conditions. For each trial, the restrainer was held above a water bath containing 50°C water and lowered by an experimenter until the tail was submerged 3-5cm. Once the mouse made a clear attempt to withdraw its tail or 10 seconds elapsed, the restrainer was raised to fully remove the tail from the water. The second trial was conducted 15-20s after the first immersion. One hour after the first test, a second set of two trials was conducted. On sets where photoinhibition was given, a laser (589nm, constant, 5mW measured at the patch cable) was turned on immediately before the first tail immersion and was left on for the duration of both trials. The order in which animal received light on and off sets was counterbalanced across animals. All trials were video recorded and manually scored in a frame-by-frame manner for the time between tail immersion and the beginning of the tail flick. Video was scored separately by two experimenters and the values from each were averaged together.

Optogenetic manipulations during two-bottle choice:
Optogenetic inhibition experiments: Behavioral testing was performed in a standard soundproof Skinner box (Med Associates). Some of the animals used for these experiments had prior behavior experience in the assays described above. However, importantly, they did not have any prior experience with alcohol. Each chamber was equipped with two bottles, and licks on both were measured via an electrical lickometer (Med Associates). Bottle placement was counterbalanced across days throughout the experiment. Initially, to train animals to drink from the lickometer, bottles contained either water or a 15% alcohol+10% sucrose solution. Mice were allowed access until 500 licks were recorded on the alcohol+sucrose lickometer. When this acquisition criterion was met, the training session was terminated (this typically occurred in less than 3 hours).

After reaching criterion, sessions were limited to one hour, and one session was performed each day. During baseline sessions (day 1-3), one bottle contained water and the other contained 15% alcohol. After three baseline sessions, increasing concentrations of quinine (250, 375, 500, 750, 1000µM) were added to the alcohol bottles during the five test days. Contact with either the water or alcohol lickometer triggered a laser on period (5s constant 589nm yellow light, 5mW light power measured at the tips of the optic fibers).

For the shock experiment, a separate cohort of animals was tested. The setup of the boxes and the experimental design was identical to that of the quinine experiment except that during the test days, increasing shock amplitudes were delivered following contacts on the alcohol lickometer. Shock amplitude was presented in ascending order across days.

Optogenetic excitation experiments: For the photoactivation experiments we used a similar two-bottle choice procedure as described above, but no punishment was paired with drinking. Instead, we tested if photoactivation was capable of producing similar behavioral effects to that of a traditional punishment. The setup of the boxes and the experimental design for the training and baseline days was identical to that of the optogenetic inhibition experiment. During the test days, lick onset at either the alcohol or water spout triggered 5s of blue light excitation (20Hz pulse, 479nm blue light), with increasing light intensity across days (10mW/mm^2 on day 4 to 130 mW/mm^2 on day 7) to establish a light power response curve. Mice were then allowed to access to alcohol and water for 5 recovery sessions were no photostimulation was delivered. Neither the water nor the alcohol bottle was adulterated with quinine at any point during this experiment.

Microstructure Analysis: Microstructure analysis of lick contacts was conducted using custom MATLAB code. The following definitions were used in the analysis, based on previous literature (*49*, *50*). The inter-lick interval was defined as the time between two lick onsets. The lick duration was defined as the time between lick onset and offset. A bout was defined as 3 licks within 1 second of each other, with the onset of the bout being the first of the 3 licks. Bout termination occurred when there was a 3 second pause in licking. Bout size was defined as the number of licks in a bout. Bout duration was defined as the length of a bout in seconds. Interbout interval was defined as the time between two bouts. Bout size, duration, and interbout interval were averaged across all the bouts in a single session for every animal. This analysis was performed on data from the photoactivation experiments; we were not able to perform this analysis on the data from the inhibition experiments due to the low number of licks following punishment in the eYFP control animals.

Extinction of operant alcohol self-administration: Testing was performed in a standard soundproof Skinner box. Each box was equipped with two nose-poke ports at either side of the box (active and inactive) and a reward port equidistant from both ports. A beam break was placed at the lickometer port to record port entries. Responses in the active nose-poke was reinforced on a fixed-ratio 1 schedule. Responses resulted in delivery of 10µl of solution, concomitant with illumination of a cue light above the reward

port. Placement of the active and inactive ports was counterbalanced across animals. A one hour session was performed each day.

During training, responses were reinforced by delivery of a 15% alcohol+10% sucrose solution until acquisition criteria was met for 3 consecutive days (minimum 20 deliveries, >75% responding on the active lever). Mice that did not meet the acquisition criteria within 10 sessions were removed from the study. Once criteria were met, animals began the maintenance phase. During the maintenance sessions, animals were allowed to self-administer a 15% alcohol solution, without sucrose, under the same conditions. Animals were allowed to self-administer for 1-hour sessions for five days, followed by two days of forced abstinence where no behavioral testing was performed. This one-week cycle was then repeated (thus animals completed a total of 10 self-administration sessions). Next, animals were tested in 10 consecutive extinction sessions during which pokes at the 'active' port had no consequence. During these sessions, reward port entry was paired with 5 seconds of yellow laser illumination (589nm, 5mW).

Histology: Subjects were deeply anaesthetized with sodium pentobarbital (200 mg kg−1; intraperitoneal injection) and transcardially perfused with 10 mL of Ringer's solution followed by 10 mL of cold 4% PFA dissolved in 1× PBS. Animals were decapitated and the brain was extracted from the cranial cavity and placed in 4% PFA solution and stored at 4 °C for at least 48-hours. Before tissue sectioning, brains were transferred to 30% sucrose solution dissolved in 1× PBS at room temperature and allowed to sit until brains sank to the bottom of the solution. Upon sinking, brains were sectioned at 50 µm on a freezing sliding microtome (HM420; Thermo Fisher Scientific). Sections were stored in 1× PBS at 4 °C until immunohistochemical processing. Sections were mounted on glass microscope slides with PVA-DABCO and stored at room temperature.

Fluorescent images were captured using a confocal laser scanning microscope (Olympus FV1000), with FluoView software (Olympus), under a dry 10× / 0.40-NA objective, a 60×/1.42-NA oil-immersion objective, or a 40× /1.30-NA oil-immersion objective. The locations of opsin expression, injection site, and optic fibers or GRIN lens were determined by taking serial z-stack images.

Statistics

Statistical analyses were performed using GraphPad Prism (GraphPad Software V6, Inc, La Jolla, CA) and MATLAB (Mathworks, Natick, MA). Comparisons across three or more variables were made using one-way ANOVAs (followed by Tukey's post-hoc test) or two-way ANOVAs (followed by Bonferroni post-hoc tests). Paired or unpaired two-tailed Student's t-tests were used to compare two variables. Two-tailed one-sample t-tests were used to compare single variables to a hypothetic mean. Thresholds for significance was placed at $p < 0.05$. All data are shown as mean ± standard error of the mean (SEM).

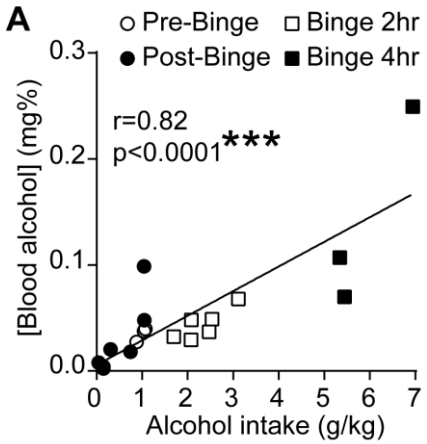

Fig. S1. Inferred alcohol consumption is positively correlated with blood alcohol concentration. (A) Alcohol intake inferred from trials completed (Pre- and Post-Binge conditioning sessions) and from differences in bottle weight (Binge Drinking sessions) positively correlated with blood alcohol concentrations, demonstrating that these are reliable measures of alcohol consumption (Pearson's correlation, r=0.82, ***p<0.0001).

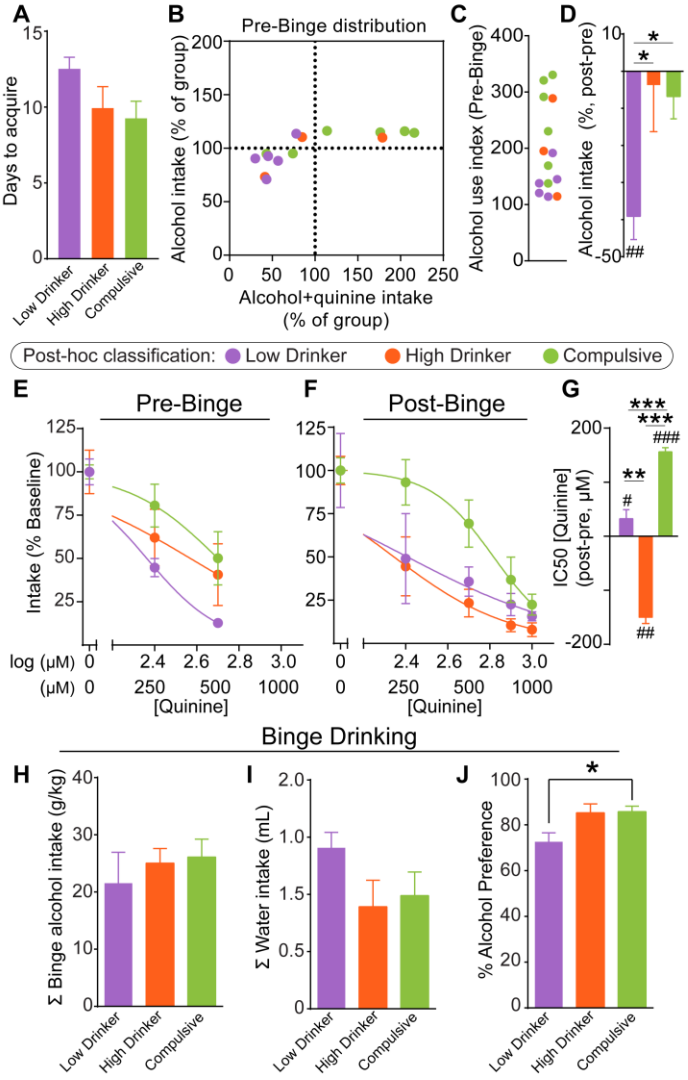

Fig. S2. Characterization of Binge-Induced Compulsion Task. (A) Number of sessions required to meet acquisition criteria did not differ between drinking phenotypes (one-way ANOVA, $F_{(2,11)}$=2.264, p=0.15). **(B)** Normalized distributions of Alcohol consumption and Alcohol+quinine during Pre-Binge conditioning sessions (group attribution from Post-Binge data in main Figure 1 was retained). **(C)** An 'alcohol use index' was calculated for each animal by summing the values from the y (Alcohol intake) and x (Alcohol+quinine intake) axes of the Pre-Binge normalized distributions. **(D)** Calculation of the difference between Post-Binge and Pre-Binge (one sample t-test against hypothetical mean of 0; Low Drinkers t_4=6.221, ##p=0.003, High Drinkers t_2=0.2943, p=0.7962, Compulsive t_5=1.137, p=0.3069). Difference scores for Low Drinkers were decreased compared to High Drinkers and Compulsive animals (one-way ANOVA, $F_{(2,11)}$=6.987, p=0.011; Tukey's post-hoc test: Low Drinkers vs. High Drinkers *p<0.05, Low Drinkers vs. Compulsive *p<0.05). **(E-F)** Alcohol intake during quinine sessions calculated as a percent of intake during non-quinine sessions for **(E)** Pre-Binge and **(F)** Post-Binge conditioning sessions. Curves were fitted with a non-linear regression to determine IC_{50} values presented in main Figure 1. **(G)** The difference

between Post-Binge and Pre-Binge IC_{50} values showed a divergence among groups (one-way ANOVA, $F_{(2, 11)}$=612.2, p<0.0001; Tukey's post-hoc test: Low Drinkers vs High Drinkers ***p<0.0001, Low Drinkers vs Compulsive ***p<0.0001, High Drinkers vs Compulsive ***p<0.0001) as Compulsive animals showed decreased sensitivity to quinine, while High Drinkers showed increased sensitivity to quinine's effects on alcohol intake following Binge Drinking (one sample t-test against hypothetical mean of 0; Low Drinkers t_4=4.317, #p=0.0125, High Drinkers t_2=22.00, ##p=0.0021, Compulsive t_5=50.32, ###p<0.0001). **(H)** Despite differences between phenotypes during conditioning and punishment (Fig. 1B-H), there were no differences in the amount of alcohol consumed during Binge Drinking (one-way ANOVA, $F_{(2,11)}$=0.332, p=0.73), suggesting that the impact of Binge Drinking on future drinking behaviors involves interactions with preexisting factors rather than the total amount of exposure per se. **(I)** Groups did not differ in total water consumed across all Binge Drinking sessions (one-way ANOVA, $F_{(2,11)}$=1.865, p=0.20). **(J)** Compulsive animals showed greater preference for alcohol over water than Low Drinkers (one-way ANOVA, $F_{(2,11)}$=5.369, p=0.02; Tukey's post-hoc test: Low Drinkers vs Compulsive *p<0.05).

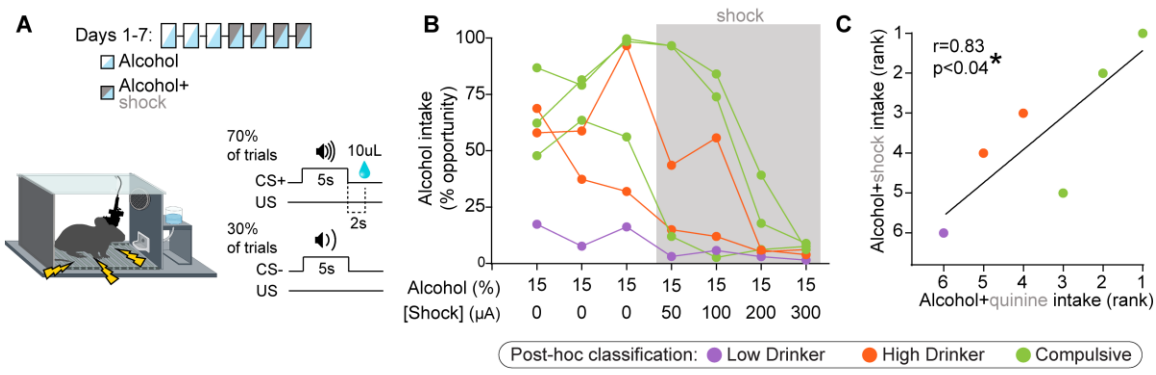

Fig. S3. Animals show persistent drinking phenotypes which are insensitive to time, context, and modality of punishment. To determine if phenotypic differences in drinking when quinine was presented reflected responses to punishment in general, as opposed to quinine-specific sensory features or habituation to quinine over sessions, a subset of animals were re-tested more than two months after completion of the Binge-Induced Compulsion Task. Animals were re-tested under identical experimental parameters, but the task was performed in a distinct context and instead of quinine punishment, alcohol consumption was punished by the delivery of a foot shock. **(A)** Experimental timeline. A subset of animals from the Binge-Induced Compulsion Task (main Figure 1) were retested ~70 days later to determine if the observed phenotypes were reproducible. Animals were tested in a different operant chamber with a similar setup, and during punishment sessions alcohol drinking resulted in delivery of a foot shock, instead of quinine punishment. **(B)** Individual animals' consumption across sessions. **(C)** There was a correlation between rank of average intakes of Alcohol+quinine and Alcohol+shock, demonstrating that animals' sensitivity to punishment is independent of punishment modality (Pearson correlation, $r=0.83$, $p<0.04$).

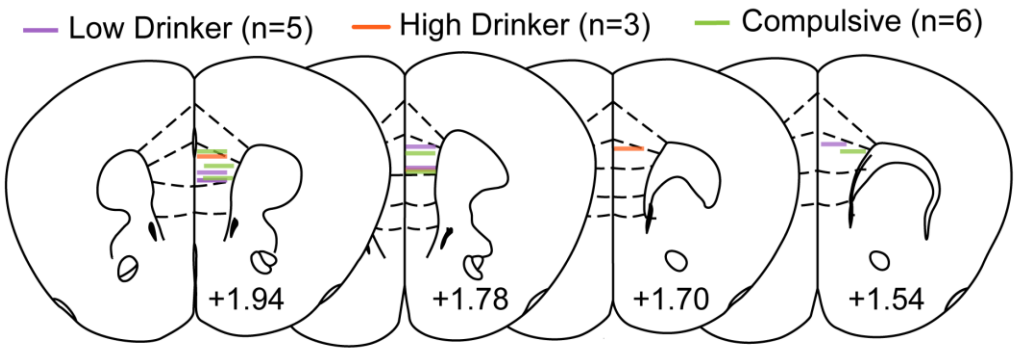

Fig. S4. Histologically verified locations of implanted GRIN lenses. Unilateral GRIN lens implant locations in the mPFC.

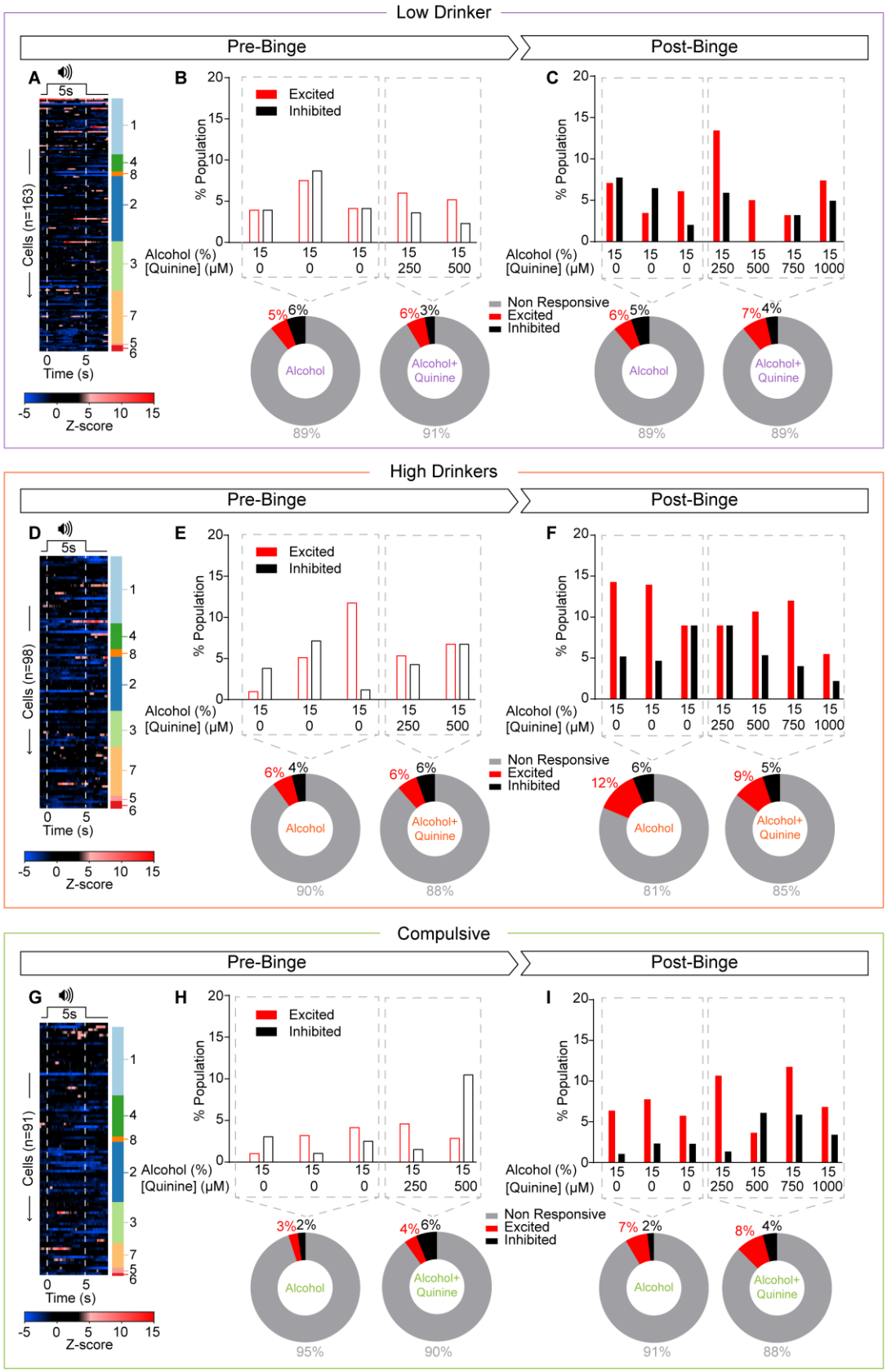
Low Drinker
Pre-Binge
Post-Binge
A
5s
Cells (n=163)
Time (s)
Z-score
B
Excited
Inhibited
% Population
Alcohol (%)
[Quinine] (μM)
C
Non Responsive
Excited
Inhibited
Alcohol
Alcohol+ Quinine
High Drinkers
D
Cells (n=98)
E
F
Compulsive
G
Cells (n=91)
H
I

Fig. S5. CS+ evoked mPFC-dPAG neuron activity before and after Binge Drinking. Comparison of cue-responses across Low Drinkers, High Drinkers and Compulsive animals. **(A-C)** No detectable differences were observed between the Pre-Binge and Post-Binge responses to the CS+ in Low Drinkers. **(A)** Heatmaps of z-scored activity of single neurons aligned around CS+ onset and averaged across trials during day 1 of Pre-Binge. Cluster designation for each neuron is shown in the bars on the right of each heatmap (clustering based on responses to alcohol show in main Figure 2 were retained). **(B)** Top: percent CS+ excited or inhibited neurons across all Pre-Binge days for Low Drinkers. Bottom: average of Alcohol only days and Alcohol+quinine days. **(C)** Top: percent CS+ excited or inhibited neurons across all Post-Binge days for Low Drinkers. Bottom: average of Alcohol only days and Alcohol+quinine days. **(D-F)** The proportion of neurons excited to the CS+ doubled from Pre-Binge (6%) to Post-Binge (12%) in High Drinkers for Alcohol Only sessions, but only increased by 50% from Pre-Binge (6%) to Post-Binge (9%) for Alcohol+quinine sessions. **(D)** Heatmaps of z-scored activity of single neurons aligned around CS+ onset and averaged across trials during day 1 of Pre-Binge. Cluster designation for each neuron is shown in the bars on the right of each heatmap (clustering based on responses to alcohol shown in main Figure 2 were retained). **(E)** Top: percent CS+ excited or inhibited neurons across all Pre-Binge days for High Drinkers. Bottom: average of Alcohol only days and Alcohol+quinine days. **(F)** Top: percent CS+ excited or inhibited neurons across all Post-Binge days for High Drinkers. Bottom: average of Alcohol only days and Alcohol+quinine days. **(G-I)** For Compulsive Drinkers, the proportion of mPFC-dPAG neurons excited to the CS+ increased by 133% from Pre-Binge (3%) to Post-Binge (7%) for Alcohol Only sessions, and increased by 100% from Pre-Binge (4%) to Post-Binge (8%) for Alcohol+quinine sessions. **(G)** Heatmaps of z-scored activity of single neurons aligned around CS+ onset and averaged across trials during day 1 of Pre-Binge. Cluster designation for each neuron is shown in the bars on the right of each heatmap (clustering based on responses to alcohol shown in main Figure 2 were retained). **(H)** Top: percent CS+ excited or inhibited neurons across all Pre-Binge days for Compulsive animals. Bottom: average of Alcohol only days and Alcohol+quinine days. **(F)** Top: percent CS+ excited or inhibited neurons across all Post-Binge days for Compulsive animals. Bottom: average of Alcohol only days and Alcohol+quinine days.

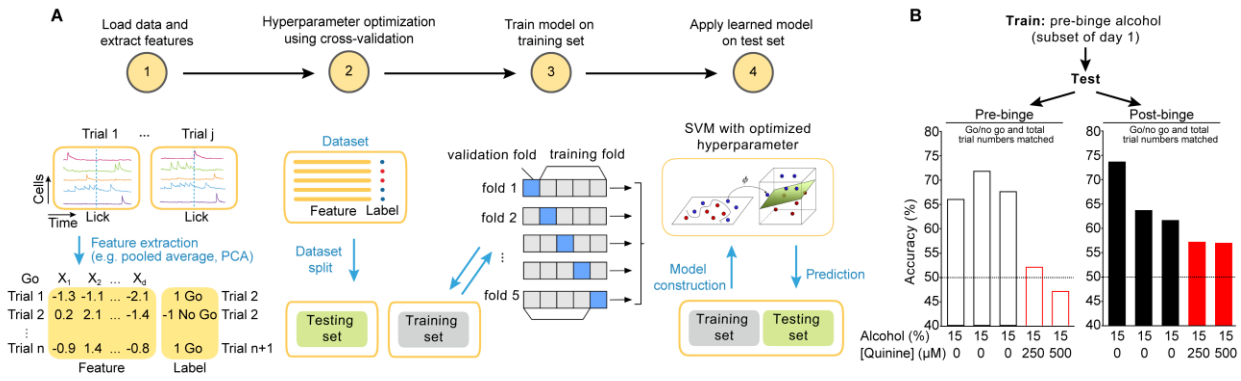

Fig. S6. mPFC-dPAG encoding during alcohol consumption influences the probability of drinking on the subsequent trial. (A) Schematic for decoder construction (adapted with permission from(*40*)). We reasoned that if activity in these neurons was updating the value of unconditioned stimuli, then activity during alcohol consumption on a given trial would influence the probability of consuming alcohol on the subsequent trial. We aimed to determine if ensemble dynamics in mPFC-dPAG neurons during the consumption of alcohol in a given trial encode the animal's decision (Go/No Go) on the subsequent trial. Pipeline: **(1)** Calcium traces were loaded. Cell and trial number varied between animals and sessions. For each cell at a given trial, calcium activity was aligned around the first lick for alcohol. An example dataset of a behavioral session from one animal consisted of *j* trials is shown. We extracted features of the neural ensemble for each trial by reducing the dimensions along cell population as well as time. Each trial was given a label based on the animal's behavior on the subsequent CS+ trial. We used a binary labeling system: 1 for Go (i.e. the animal consumed alcohol on the subsequent opportunity) and -1 for NoGo (i.e. the animal did not consume alcohol on the subsequent opportunity). We then combined data across all animals and trials to construct a full dataset with *n* features and *n* labels, where *n* was the number of all the trials across animals and sessions. **(2)** Next, we split our full dataset into a training set (a subset of day 1 pre-binge data, see methods) and testing sets (all remaining data). We then optimized hyper-parameters of the decoder (see methods for details) using a 5-fold cross-validation within the training set. **(3)** After optimization, we re-trained the decoder based on the full training set. **(4)** Finally, we applied the trained model on testing sets to obtain a decoding accuracy. **(B)** Decoding performance Pre-Binge and Post-Binge. The decoder is trained using a subset of Pre-Binge data taken from Day 1, and tested on different days across the paradigm (for Pre-Binge day 1, the testing set was a subset of trials that was not included in the training set). Left: decoding performance on Pre-Binge days. The decoding performance is above 65% and remains similar when tested across days without quinine. However, performance drops when tested on sessions with quinine added, suggesting that mPFC-dPAG neurons use a different coding rule for punished trials. Right: decoding performance on Post-Binge days. The decoding performance is above 60% on Alcohol sessions despite being trained on data collected more than 2 weeks prior. Similar to Pre-Binge data, accuracy drops when tested on Alcohol+quinine sessions, albeit to a lesser extent.

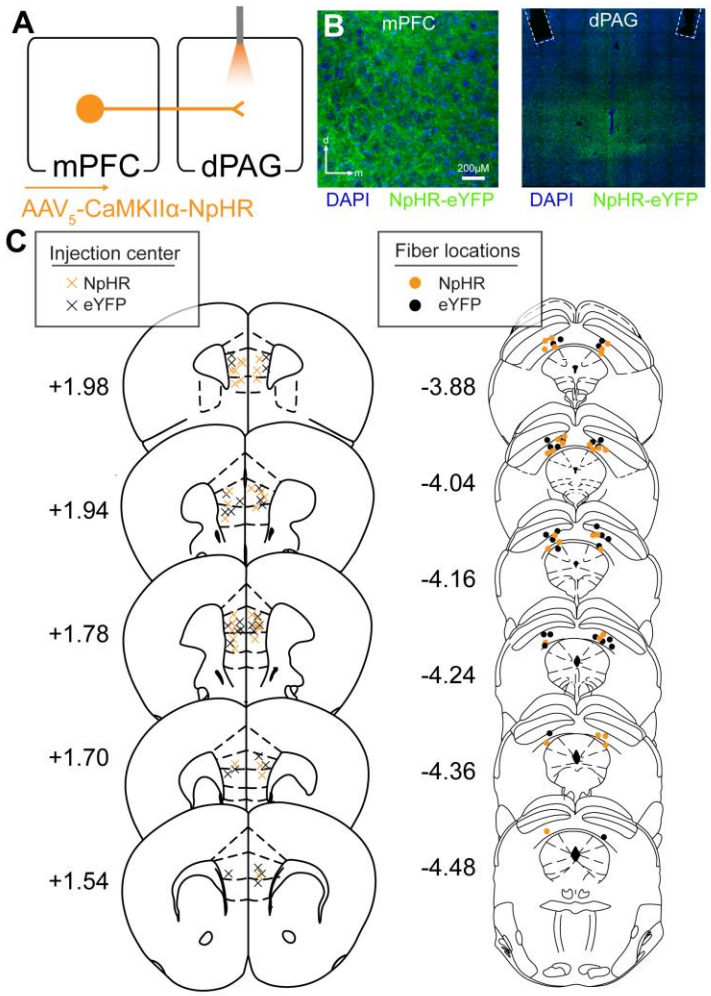

Fig. S7. Histological verification of viral expression and fiber placement for optogenetic inhibition of mPFC-dPAG terminals. (A) Viral transduction strategy to allow optogenetic inhibition of mPFC-dPAG neurons. **(B)** Representative histological image. **(C)** Bilateral virus injection locations in the mPFC and optic fiber implants above the dPAG for NpHR- and eYFP-expressing mice.

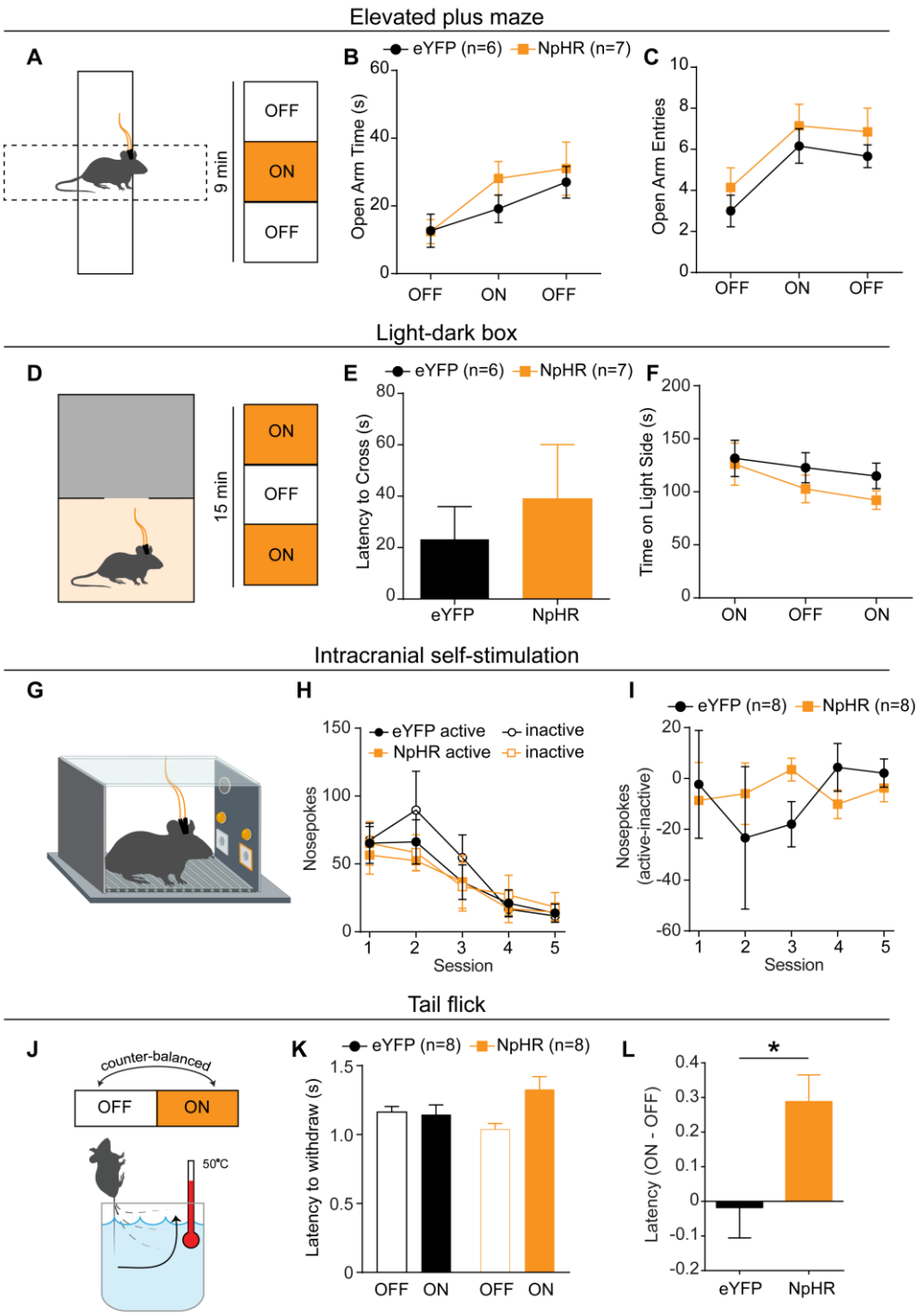

Fig. S8. Optogenetic inhibition of mPFC terminals in the dPAG does not alter anxiety-related behavior or produce intracranial self-stimulation, but increases latency to withdraw from hot water. (A) Left: schematic of behavioral apparatus. Right: timeline of optogenetic manipulations during exploration of an elevated plus maze consisting of 3 minute epochs (OFF-ON-OFF). During the ON epochs, light was

delivered continuously throughout. **(B)** There was no difference in open arm time between groups (two-way mixed-design ANOVA (Group x Epoch), group: $F_{(1,11)}$=0.505, p=0.49, epoch: $F_{(2,22)}$=9.12, **p=0.001). **(C)** There was no difference in open arm entries between groups (two-way mixed-design ANOVA (Group x Epoch), group: $F_{(1,11)}$=1.031, p=0.33, epoch: $F_{(2,22)}$=12.74, ***p=0.0002). **(D)** Left: schematic of behavioral apparatus. Right: timeline of optogenetic manipulations during exploration of a light-dark box consisting of 5 minute epochs (ON-OFF-ON). During ON epochs, light was delivered continuously throughout. **(E)** Animals were placed on the light side of the box, and latency to cross to the dark side was determined. Photoinhibition did not alter latency to cross (unpaired t-test, t_{11}=0.612, p=0.55). **(F)** Total time spent on the light side throughout the epochs did not differ between groups (two-way mixed-design ANOVA (Group x Epoch), group: $F_{(1,11)}$=1.315, p=0.28, epoch: $F_{(2,22)}$=1.845, p=0.18). **(G)** Experimental schematic for intracranial self-stimulation. Initiation of the active nose-poke resulted in illumination of a cue light, an auditory tone, and a 5 second laser on period. The inactive nose-poke resulted in illumination of a cue light and a distinct auditory tone, but no light was delivered. **(H)** Active and inactive nose-pokes over 5 sessions. **(I)** Active minus inactive nose-pokes did not differ between groups (two-way mixed-design ANOVA (Group x Epoch), group: $F_{(1,69)}$=0.081, p=0.78, epoch: $F_{(4,69)}$=0.32, p=0.87). **(J)** Experimental schematic for tail flick assay. Animals were placed in a restrainer and their tails were dipped into 50°C water under either light ON or light OFF conditions. **(K)** Latency to tail flick across groups and conditions. **(L)** Difference score (on minus off) was greater in NpHR animals, indicating that inhibition slowed tail flick response (unpaired t-test, t_{14}=2.623, p=0.02).

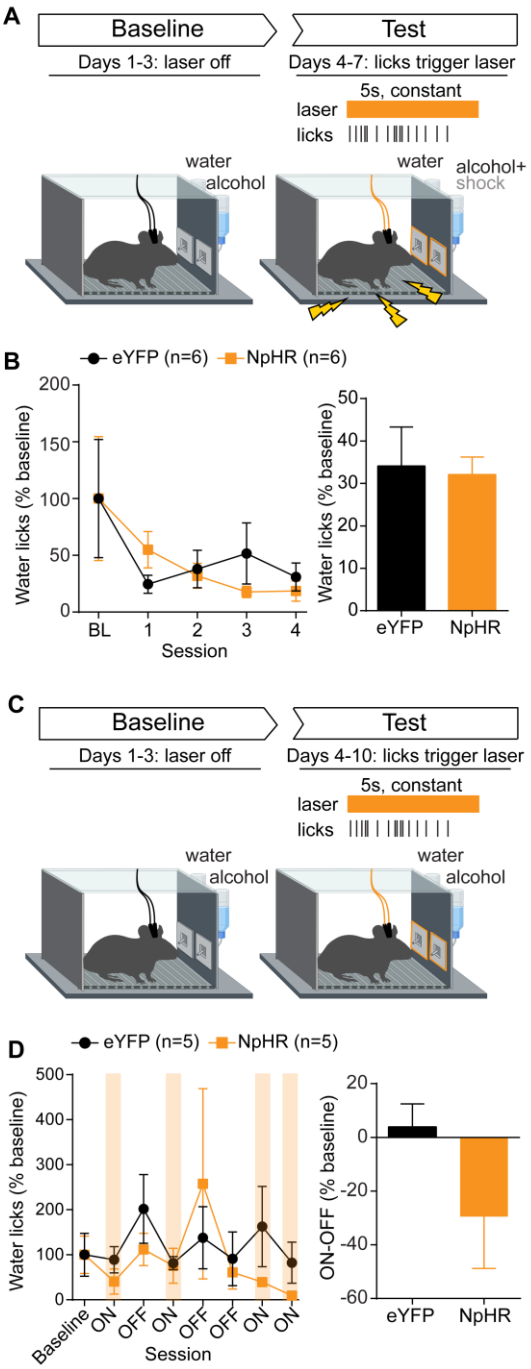

Fig. S9. Inhibition of mPFC-dPAG terminals does not alter water consumption. (A) Experimental timeline for assessing the effect of mPFC-dPAG terminal inhibition on alcohol drinking punished with shock. Licks on the alcohol spout are presented in main Figure 3. **(B)** Left: licks on the water spout during each laser on session as a percent of baseline. Right: total licks during laser on sessions as a percent of baseline show no difference in licking for water between groups (unpaired t-test, t_{10}=0.198, p=0.85). **(C)** Experimental timeline for assessing the effect of mPFC-dPAG terminal inhibition on

alcohol drinking in the absence of punishment. Licks on the alcohol spout are presented in main Figure 3. **(D)** Left: licks on the water spout during each laser on session as a percent of baseline. Right: total licks during laser on sessions as a percent of baseline show no difference in licking for water between groups (unpaired t-test, t_8=1.58, p=0.15).

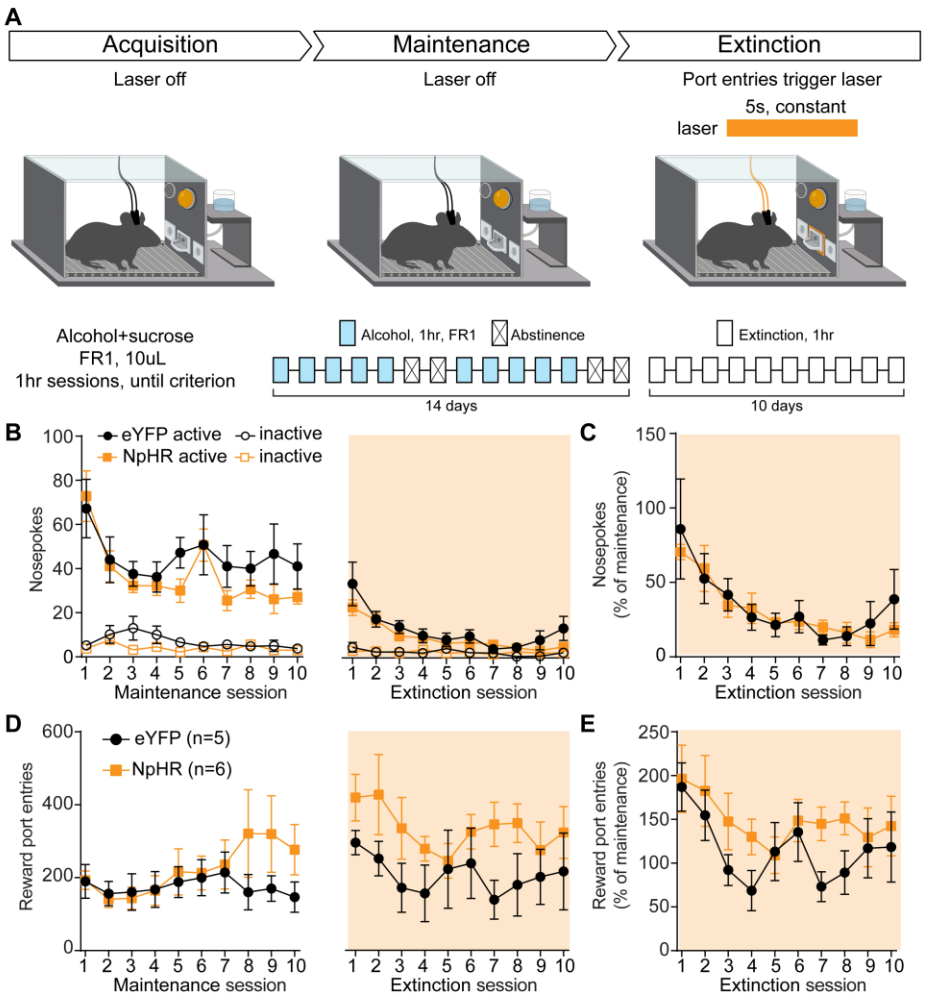

Fig. S10. Optogenetic inhibition of mPFC-dPAG terminals does not alter extinction of operant responding for alcohol. (A) Experimental timeline for assessing the effect of mPFC-dPAG terminal inhibition on extinction of operant alcohol self-administration. During acquisition, behavior was reinforced with a 10% sucrose + 15% alcohol (v/v) solution delivered on a fixed-ratio 1 schedule. Once acquisition criteria were met, sucrose was removed and animals were allowed to self-administer 15% alcohol on a fixed ratio 1 schedule for 5 days per week for 2 weeks (maintenance phase), before entering the extinction phase. During extinction, both active and inactive nose-pokes had no programed consequence. Also beginning in the extinction phase, entries into the reward port triggered a 5 second laser on period. **(B)** Left: responding on the active and inactive nose-poke during self-administration. Right: responding on the active and inactive nose-poke during extinction. **(C)** Active nose-poke responses during extinction normalized to the average responding during the final week of self-administration for each animal showed that responding changed over extinction sessions, but did not differ between groups (two-way mixed-design ANOVA (Group x Session), group: $F_{(1,9)}$=0.114, p=0.74, session: $F_{(9,81)}$=8.142, ***p<0.0001). **(D)** Reward port entries during self-administration (left) or extinction (right). **(E)** Reward port entries during extinction normalized to the average entries during the final week of self-

administration for each animal showed no differences between groups (two-way mixed-design ANOVA (Group x Session), group: $F_{(1,9)}$=1.398, p=0.27, session: $F_{(9,81)}$=3.183, **p=0.002).

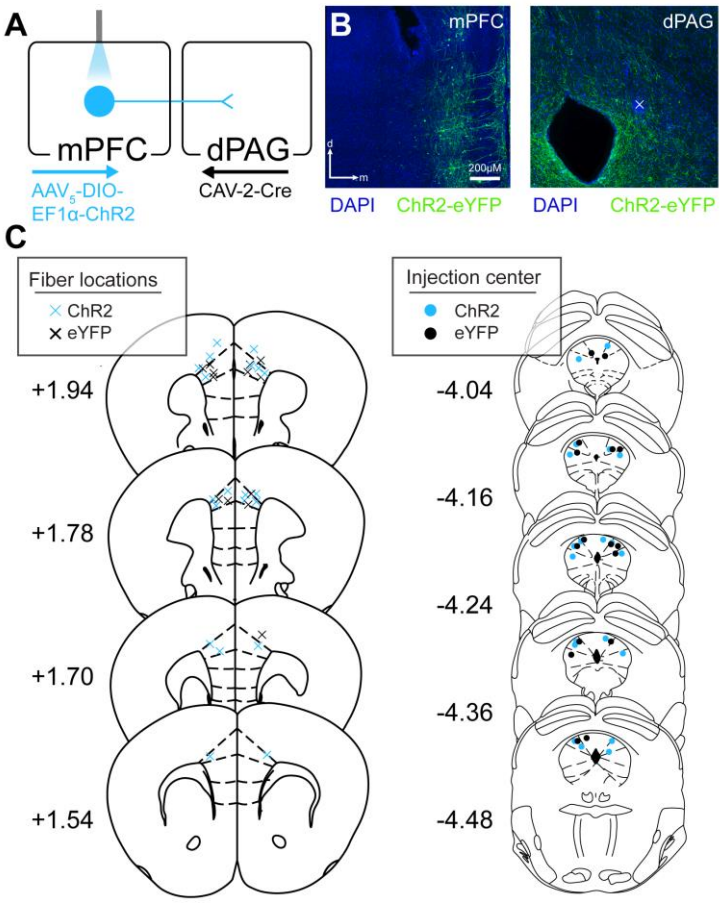

Fig. S11. Histological verification of virus injection and fiber placement for optogenetic activation of mPFC-dPAG neurons. (A) Viral transduction strategy to allow optogenetic activation of mPFC-dPAG neurons. **(B)** Representative histological image. **(C)** Bilateral optical-fiber implant locations above the mPFC and virus injection locations in the dPAG for ChR2- and eYFP-expressing mice.

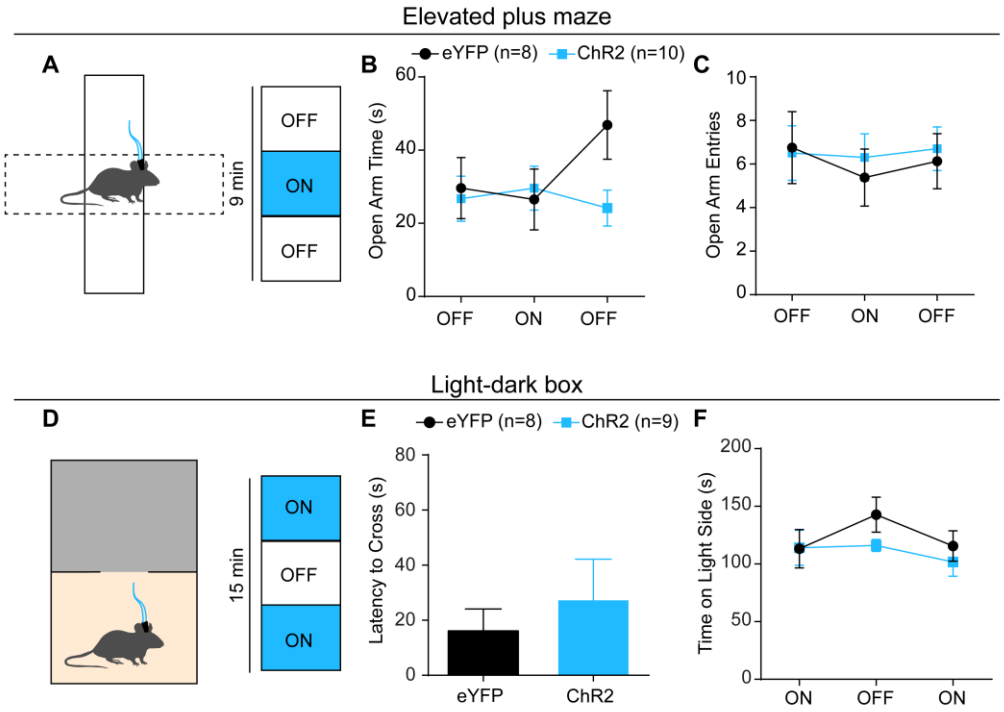

Fig. S12. Optogenetic activation of mPFC-dPAG neurons does not alter anxiety-related behavior in elevated plus maze or light-dark box assays. (A) Left: schematic of behavioral apparatus. Right: timeline of optogenetic manipulations during exploration of an elevated plus maze consisting of 3 minute epochs (OFF-ON-OFF). During the ON epoch, light was delivered at 20 Hz throughout. **(B)** There was no difference in open arm time between groups (two-way mixed-design ANOVA (Group x Epoch), group: $F_{(1,16)}$= 0.713, p=0.41, epoch: $F_{(2,32)}$=2.223, p=0.12). **(C)** There was no difference in open arm entries between groups (two-way mixed-design ANOVA (Group x Epoch), group: $F_{(1,16)}$= 0.077, p=0.79, epoch: $F_{(2,32)}$=0.483, p=0.62). **(D)** Left: schematic of behavioral apparatus. Right: timeline of optogenetic manipulations during exploration of a light-dark box consisting of 5 minute epochs (ON-OFF-ON). During ON epochs, light was delivered at 20 Hz throughout. **(E)** Animals were placed on the light side of the box, and latency to cross to the dark side was determined. Photoactivation did not alter latency to cross (unpaired t-test, t_{15}=0.66, p=0.52). **(F)** Total time spent on the light side throughout the epochs did not differ between groups (two-way mixed-design ANOVA (Group x Epoch), group: $F_{(1,15)}$= 0.835, p=0.38, epoch: $F_{(2,30)}$=2.143, p=0.14).

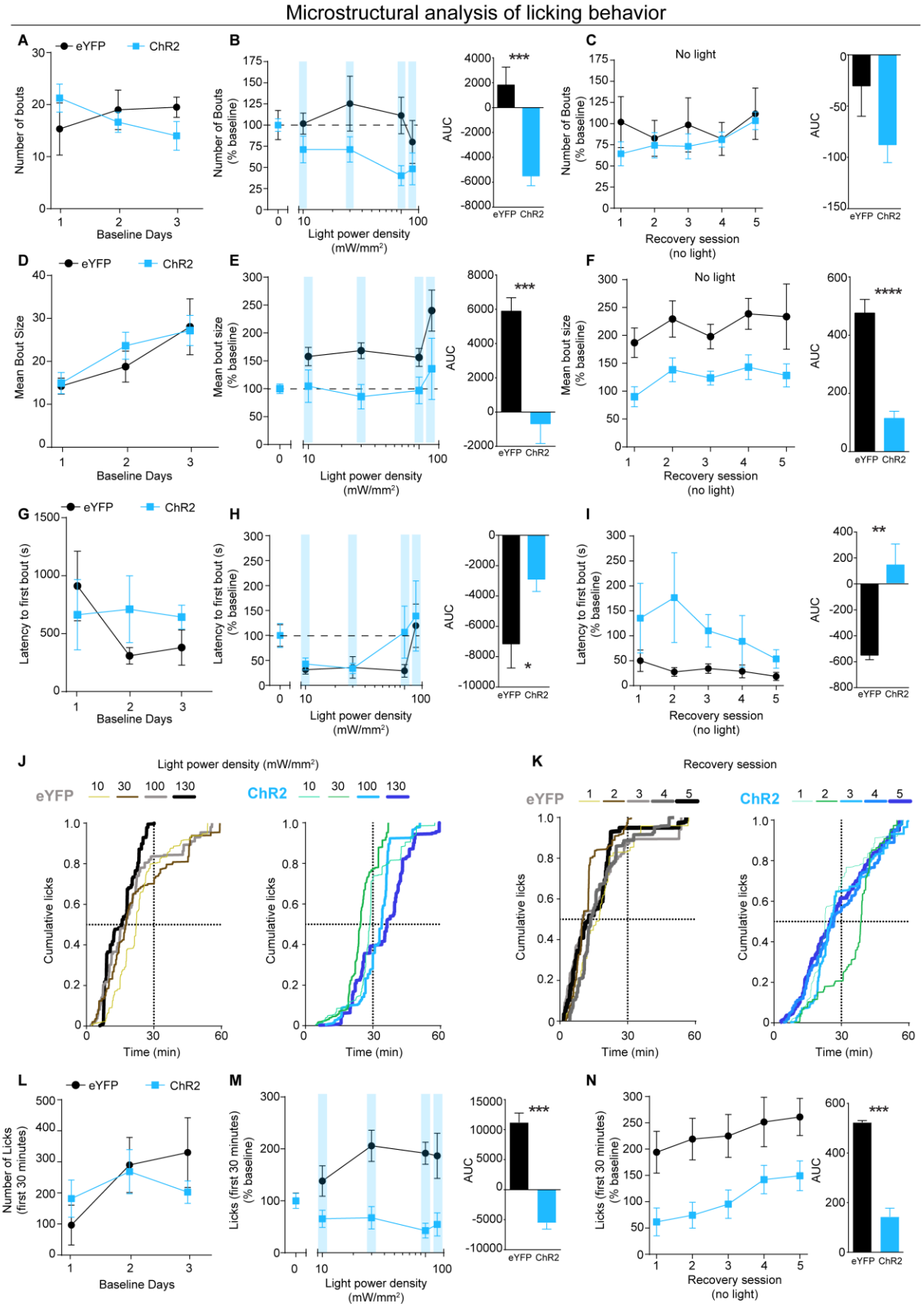
Microstructural analysis of licking behavior
A
eYFP
ChR2
Number of bouts
Baseline Days
B
Number of Bouts (% baseline)
Light power density (mW/mm²)
AUC
***
eYFP ChR2
C
No light
Number of Bouts (% baseline)
Recovery session (no light)
AUC
eYFP ChR2
D
Mean Bout Size
Baseline Days
E
Mean bout size (% baseline)
Light power density (mW/mm²)
AUC
***
eYFP ChR2
F
No light
Mean bout size (% baseline)
Recovery session (no light)
AUC
****
eYFP ChR2
G
Latency to first bout (s)
Baseline Days
H
Latency to first bout (s) (% baseline)
Light power density (mW/mm²)
AUC
*
eYFP ChR2
I
Latency to first bout (s) (% baseline)
Recovery session (no light)
AUC
**
eYFP ChR2
J
Light power density (mW/mm²)
eYFP 10 30 100 130
ChR2 10 30 100 130
Cumulative licks
Time (min)
K
Recovery session
eYFP 1 2 3 4 5
ChR2 1 2 3 4 5
Cumulative licks
Time (min)
L
Number of Licks (first 30 minutes)
Baseline Days
M
Licks (first 30 minutes) (% baseline)
Light power density (mW/mm²)
AUC
***
eYFP ChR2
N
Licks (first 30 minutes) (% baseline)
Recovery session (no light)
AUC
***
eYFP ChR2

Fig. S13. Optogenetic activation of mPFC-dPAG neurons during alcohol consumption alters microstructure of licking behavior. (A) Number of lick bouts for alcohol did not differ between ChR2 and eYFP animals during the baseline sessions (repeated measures two-way ANOVA, no main effect of group, $F_{(1,12)}$=0.04619, p=0.83). **(B)** Left: licks bouts on the alcohol spout during each light on session as a percent of baseline. Right: area under the light power density curve for lick bouts was decreased in ChR2 animals as compared to eYFP controls (two-tailed unpaired t-test, t_{12}=4.784, ***p=0.0004). **(C)** Left: licks bouts on the alcohol spout during each recovery session as a percent of baseline. Right: area under the curve for lick bouts during recovery sessions did not differ between ChR2 and eYFP animals (two-tailed unpaired t-test, t_{12}=1.767, p=0.10). **(D)** Bout size (average number of licks per bout) for alcohol increased over days during the baseline sessions (repeated measures two-way ANOVA, main effect of session, $F_{(2, 24)}$=5.202, *p=0.01), but did not differ between ChR2 and eYFP animals (no main effect of group, $F_{(1, 12)}$=0.4604, p=0.51). **(E)** Left: bout size on the alcohol spout during each light on session as a percent of baseline. Right: area under the light power density curve for bout size was decreased in ChR2 animals as compared to eYFP controls (two-tailed unpaired t-test, t_{12}=4.360, ***p=0.0009). **(F)** Left: bouts size on the alcohol spout during each recovery session as a percent of baseline. Right: area under the curve for bout size during recovery sessions was decreased in ChR2 animals as compared to eYFP controls (two-tailed unpaired t-test, t_{12}=7.353, ***p<0.0001). **(G)** Latency to first lick bout on the alcohol spout did not differ between ChR2 and eYFP animals during baseline sessions (repeated measures two-way ANOVA, no main effect of group, $F_{(1,12)}$= 0.4234, p=0.53). **(H)** Left: latency to initiate the first bout on the alcohol spout during each light on session as a percent of baseline. Right: area under the light power density curve for latency to initiate first bout was increased in ChR2 animals as compared to eYFP controls, indicating longer latencies to begin drinking (two-tailed unpaired t-test, t_{12}=2.586, *p=0.0238). **(I)** Left: latency to initiate the first bout on the alcohol spout during each recovery session as a percent of baseline. Right: area under the curve for latency to initiate first bout during recovery sessions was increased in ChR2 animals as compared to eYFP controls (two-tailed unpaired t-test, t_{12}=3.614, **p=0.0036). **(J)** Cumulative normalized response curves illustrating timing of licks throughout the hour-long sessions for population averages of eYFP (left) and ChR2 (right) groups across test days. **(K)** Cumulative normalized response curves for population averages of eYFP (left) and ChR2 (right) groups across recovery days. **(L)** Number of licks during the first 30 minutes of each baseline session did not differ between groups (repeated measures two-way ANOVA, no main effect of group, $F_{(1,12)}$=0.1977, p=0.67). **(M)** Left: licks on the alcohol spout in the first 30 minutes of each session for each light on session as a percent of baseline. Right: area under the light power density curve for licks during the first 30 minutes of each session was decreased in ChR2 animals as compared to eYFP controls. **(N)** Left: licks on the alcohol spout in the first 30 minutes of each session for each recovery session as a percent of baseline. Right: area under the curve for licks on the alcohol spout in the first 30 minutes during recovery sessions was decreased in ChR2 animals as compared to eYFP controls.

References and Notes

1. Substance Abuse and Mental Health Services Administration, Center for Behavioral Health Statistics and Quality, *Results from the 2017 National Survey on Drug Use and Health: Detailed Tables* (2017); www.samhsa.gov/data/sites/default/files/cbhsq-reports/NSDUHDetailedTabs2017/NSDUHDetailedTabs2017.pdf.

2. B. F. Grant, R. B. Goldstein, T. D. Saha, S. P. Chou, J. Jung, H. Zhang, R. P. Pickering, W. J. Ruan, S. M. Smith, B. Huang, D. S. Hasin, Epidemiology of *DSM-5* Alcohol use disorder: Results from the National Epidemiologic Survey on Alcohol and Related Conditions III. *JAMA Psychiatry* **72**, 757–766 (2015). doi:10.1001/jamapsychiatry.2015.0584 Medline

3. F. W. Hopf, H. M. B. Lesscher, Rodent models for compulsive alcohol intake. *Alcohol* **48**, 253–264 (2014). doi:10.1016/j.alcohol.2014.03.001 Medline

4. L. J. M. J. Vanderschuren, B. J. Everitt, Drug seeking becomes compulsive after prolonged cocaine self-administration. *Science* **305**, 1017–1019 (2004). doi:10.1126/science.1098975 Medline

5. American Psychiatric Association, *Diagnostic and Statistical Manual of Mental Disorders* (*DSM-5*®) (American Psychiatric Association, 2013).

6. K. McFarland, C. C. Lapish, P. W. Kalivas, Prefrontal glutamate release into the core of the nucleus accumbens mediates cocaine-induced reinstatement of drug-seeking behavior. *J. Neurosci.* **23**, 3531–3537 (2003). doi:10.1523/JNEUROSCI.23-08-03531.2003 Medline

7. B. T. Chen, H.-J. Yau, C. Hatch, I. Kusumoto-Yoshida, S. L. Cho, F. W. Hopf, A. Bonci, Rescuing cocaine-induced prefrontal cortex hypoactivity prevents compulsive cocaine seeking. *Nature* **496**, 359–362 (2013). doi:10.1038/nature12024 Medline

8. G. F. Koob, N. D. Volkow, Neurocircuitry of addiction. *Neuropsychopharmacology* **35**, 217–238 (2010). doi:10.1038/npp.2009.110 Medline

9. P. W. Kalivas, N. Volkow, J. Seamans, Unmanageable motivation in addiction: A pathology in prefrontal-accumbens glutamate transmission. *Neuron* **45**, 647–650 (2005). doi:10.1016/j.neuron.2005.02.005 Medline

10. J. W. Dalley, B. J. Everitt, T. W. Robbins, Impulsivity, compulsivity, and top-down cognitive control. *Neuron* **69**, 680–694 (2011). doi:10.1016/j.neuron.2011.01.020 Medline

11. M. M. Silveri, J. Rogowska, A. McCaffrey, D. A. Yurgelun-Todd, Adolescents at risk for alcohol abuse demonstrate altered frontal lobe activation during Stroop performance. *Alcohol. Clin. Exp. Res.* **35**, 218–228 (2011). doi:10.1111/j.1530-0277.2010.01337.x Medline

12. A. D. Schweinsburg, M. P. Paulus, V. C. Barlett, L. A. Killeen, L. C. Caldwell, C. Pulido, S. A. Brown, S. F. Tapert, An FMRI study of response inhibition in youths with a family history of alcoholism. *Ann. N. Y. Acad. Sci.* **1021**, 391–394 (2004). doi:10.1196/annals.1308.050 Medline

13. O. M. Mahmood, D. Goldenberg, R. Thayer, R. Migliorini, A. N. Simmons, S. F. Tapert, Adolescents' fMRI activation to a response inhibition task predicts future substance use. *Addict. Behav.* **38**, 1435–1441 (2013). doi:10.1016/j.addbeh.2012.07.012 Medline

14. T. Seif, S.-J. Chang, J. A. Simms, S. L. Gibb, J. Dadgar, B. T. Chen, B. K. Harvey, D. Ron, R. O. Messing, A. Bonci, F. W. Hopf, Cortical activation of accumbens hyperpolarization-active NMDARs mediates aversion-resistant alcohol intake. *Nat. Neurosci.* **16**, 1094–1100 (2013). doi:10.1038/nn.3445 Medline

15. O. George, C. Sanders, J. Freiling, E. Grigoryan, S. Vu, C. D. Allen, E. Crawford, C. D. Mandyam, G. F. Koob, Recruitment of medial prefrontal cortex neurons during alcohol withdrawal predicts cognitive impairment and excessive alcohol drinking. *Proc. Natl. Acad. Sci. U.S.A.* **109**, 18156–18161 (2012). doi:10.1073/pnas.1116523109 Medline

16. A. Holmes, P. J. Fitzgerald, K. P. MacPherson, L. DeBrouse, G. Colacicco, S. M. Flynn, S. Masneuf, K. E. Pleil, C. Li, C. A. Marcinkiewcz, T. L. Kash, O. Gunduz-Cinar, M. Camp, Chronic alcohol remodels prefrontal neurons and disrupts NMDAR-mediated fear extinction encoding. *Nat. Neurosci.* **15**, 1359–1361 (2012). doi:10.1038/nn.3204 Medline

17. K. E. Pleil, E. G. Lowery-Gionta, N. A. Crowley, C. Li, C. A. Marcinkiewcz, J. H. Rose, N. M. McCall, A. M. Maldonado-Devincci, A. L. Morrow, S. R. Jones, T. L. Kash, Effects of chronic ethanol exposure on neuronal function in the prefrontal cortex and extended amygdala. *Neuropharmacology* **99**, 735–749 (2015). doi:10.1016/j.neuropharm.2015.06.017 Medline

18. D. M. Lovinger, J. C. Crabbe, Laboratory models of alcoholism: Treatment target identification and insight into mechanisms. *Nat. Neurosci.* **8**, 1471–1480 (2005). doi:10.1038/nn1581 Medline

19. C. Giuliano, Y. Peña-Oliver, C. R. Goodlett, R. N. Cardinal, T. W. Robbins, E. T. Bullmore, D. Belin, B. J. Everitt, Evidence for a long-lasting compulsive alcohol seeking phenotype in rats. *Neuropsychopharmacology* **43**, 728–738 (2018). doi:10.1038/npp.2017.105 Medline

20. M. Roberto, M. T. Cruz, N. W. Gilpin, V. Sabino, P. Schweitzer, M. Bajo, P. Cottone, S. G. Madamba, D. G. Stouffer, E. P. Zorrilla, G. F. Koob, G. R. Siggins, L. H. Parsons, Corticotropin releasing factor-induced amygdala gamma-aminobutyric Acid release plays a key role in alcohol dependence. *Biol. Psychiatry* **67**, 831–839 (2010). doi:10.1016/j.biopsych.2009.11.007 Medline

21. K. Goltseker, F. W. Hopf, S. Barak, Advances in behavioral animal models of alcohol use disorder. *Alcohol* **74**, 73–82 (2019). doi:10.1016/j.alcohol.2018.05.014 Medline

22. T. E. Thiele, M. Navarro, "Drinking in the dark" (DID) procedures: A model of binge-like ethanol drinking in non-dependent mice. *Alcohol* **48**, 235–241 (2014). doi:10.1016/j.alcohol.2013.08.005 Medline

23. T. B. Franklin, B. A. Silva, Z. Perova, L. Marrone, M. E. Masferrer, Y. Zhan, A. Kaplan, L. Greetham, V. Verrechia, A. Halman, S. Pagella, A. L. Vyssotski, A. Illarionova, V. Grinevich, T. Branco, C. T. Gross, Prefrontal cortical control of a brainstem social behavior circuit. *Nat. Neurosci.* **20**, 260–270 (2017). doi:10.1038/nn.4470 Medline

24. C. M. Vander Weele, C. A. Siciliano, G. A. Matthews, P. Namburi, E. M. Izadmehr, I. C. Espinel, E. H. Nieh, E. H. S. Schut, N. Padilla-Coreano, A. Burgos-Robles, C.-J. Chang, E. Y. Kimchi, A. Beyeler, R. Wichmann, C. P. Wildes, K. M. Tye, Dopamine enhances signal-to-noise ratio in cortical-brainstem encoding of aversive stimuli. *Nature* **563**, 397–401 (2018). doi:10.1038/s41586-018-0682-1 Medline

25. Y. Li, J. Zeng, J. Zhang, C. Yue, W. Zhong, Z. Liu, Q. Feng, M. Luo, Hypothalamic circuits for predation and evasion. *Neuron* **97**, 911–924.e5 (2018). doi:10.1016/j.neuron.2018.01.005 Medline

26. D. A. Evans, A. V. Stempel, R. Vale, S. Ruehle, Y. Lefler, T. Branco, A synaptic threshold mechanism for computing escape decisions. *Nature* **558**, 590–594 (2018). doi:10.1038/s41586-018-0244-6 Medline

27. R. R. Rozeske, D. Jercog, N. Karalis, F. Chaudun, S. Khoder, D. Girard, N. Winke, C. Herry, Prefrontal-periaqueductal gray-projecting neurons mediate context fear discrimination. *Neuron* **97**, 898–910.e6 (2018). doi:10.1016/j.neuron.2017.12.044 Medline

28. A. Cabral, N. Isoardi, C. Salum, C. E. Macedo, M. J. Nobre, V. A. Molina, M. L. Brandão, Fear state induced by ethanol withdrawal may be due to the sensitization of the neural substrates of aversion in the dPAG. *Exp. Neurol.* **200**, 200–208 (2006). doi:10.1016/j.expneurol.2006.02.004 Medline

29. E. M. Avegno, T. D. Lobell, C. A. Itoga, B. B. Baynes, A. M. Whitaker, M. M. Weera, S. Edwards, J. W. Middleton, N. W. Gilpin, Central amygdala circuits mediate hyperalgesia in alcohol-dependent rats. *J. Neurosci.* **38**, 7761–7773 (2018). doi:10.1523/JNEUROSCI.0483-18.2018 Medline

30. C. A. Siciliano, K. M. Tye, Leveraging calcium imaging to illuminate circuit dysfunction in addiction. *Alcohol* **74**, 47–63 (2019). doi:10.1016/j.alcohol.2018.05.013 Medline

31. E. J. Kremer, S. Boutin, M. Chillon, O. Danos, Canine adenovirus vectors: An alternative for adenovirus-mediated gene transfer. *J. Virol.* **74**, 505–512 (2000). doi:10.1128/JVI.74.1.505-512.2000 Medline

32. J. S. Rhodes, K. Best, J. K. Belknap, D. A. Finn, J. C. Crabbe, Evaluation of a simple model of ethanol drinking to intoxication in C57BL/6J mice. *Physiol. Behav.* **84**, 53–63 (2005). doi:10.1016/j.physbeh.2004.10.007 Medline

33. J. S. Rhodes, M. M. Ford, C.-H. Yu, L. L. Brown, D. A. Finn, T. Garland Jr., J. C. Crabbe, Mouse inbred strain differences in ethanol drinking to intoxication. *Genes Brain Behav.* **6**, 1–18 (2007). doi:10.1111/j.1601-183X.2006.00210.x Medline

34. M. V. Wilcox, V. C. Cuzon Carlson, N. Sherazee, G. M. Sprow, R. Bock, T. E. Thiele, D. M. Lovinger, V. A. Alvarez, Repeated binge-like ethanol drinking alters ethanol drinking patterns and depresses striatal GABAergic transmission. *Neuropsychopharmacology* **39**, 579–594 (2014). doi:10.1038/npp.2013.230 Medline

35. Y. Ziv, L. D. Burns, E. D. Cocker, E. O. Hamel, K. K. Ghosh, L. J. Kitch, A. El Gamal, M. J. Schnitzer, Long-term dynamics of CA1 hippocampal place codes. *Nat. Neurosci.* **16**, 264–266 (2013). doi:10.1038/nn.3329 Medline

36. K. K. Ghosh, L. D. Burns, E. D. Cocker, A. Nimmerjahn, Y. Ziv, A. E. Gamal, M. J. Schnitzer, Miniaturized integration of a fluorescence microscope. *Nat. Methods* **8**, 871–878 (2011). doi:10.1038/nmeth.1694 Medline

37. P. Zhou, S. L. Resendez, J. Rodriguez-Romaguera, J. C. Jimenez, S. Q. Neufeld, A. Giovannucci, J. Friedrich, E. A. Pnevmatikakis, G. D. Stuber, R. Hen, M. A. Kheirbek, B. L. Sabatini, R. E. Kass, L. Paninski, Efficient and accurate extraction of in vivo calcium signals from microendoscopic video data. *eLife* **7**, e28728 (2018). 10.7554/eLife.28728 Medline

38. M. Murugan, H. J. Jang, M. Park, E. M. Miller, J. Cox, J. P. Taliaferro, N. F. Parker, V. Bhave, H. Hur, Y. Liang, A. R. Nectow, J. W. Pillow, I. B. Witten, Combined social and spatial coding in a descending projection from the prefrontal cortex. *Cell* **171**, 1663–1677.e16 (2017). doi:10.1016/j.cell.2017.11.002 Medline

39. J. M. Otis, V. M. K. Namboodiri, A. M. Matan, E. S. Voets, E. P. Mohorn, O. Kosyk, J. A. McHenry, J. E. Robinson, S. L. Resendez, M. A. Rossi, G. D. Stuber, Prefrontal cortex output circuits guide reward seeking through divergent cue encoding. *Nature* **543**, 103–107 (2017). doi:10.1038/nature21376 Medline

40. C.-J. Chang, *Technical Report: Building a Neural Ensemble Decoder by Extracting Features Shared Across Multiple Populations* (MIT, 2019); https://dspace.mit.edu/bitstream/handle/1721.1/122041/Chang-Technical_Report092019.pdf?sequence=1&isAllowed=y.

41. A. M. Stamatakis, G. D. Stuber, Activation of lateral habenula inputs to the ventral midbrain promotes behavioral avoidance. *Nat. Neurosci.* **15**, 1105–1107 (2012). doi:10.1038/nn.3145 Medline

42. A. V. Kravitz, L. D. Tye, A. C. Kreitzer, Distinct roles for direct and indirect pathway striatal neurons in reinforcement. *Nat. Neurosci.* **15**, 816–818 (2012). doi:10.1038/nn.3100 Medline

43. J. Olds, P. Milner, Positive reinforcement produced by electrical stimulation of septal area and other regions of rat brain. *J. Comp. Physiol. Psychol.* **47**, 419–427 (1954). doi:10.1037/h0058775 Medline

44. G. D. Stuber, D. R. Sparta, A. M. Stamatakis, W. A. van Leeuwen, J. E. Hardjoprajitno, S. Cho, K. M. Tye, K. A. Kempadoo, F. Zhang, K. Deisseroth, A. Bonci, Excitatory transmission from the amygdala to nucleus accumbens facilitates reward seeking. *Nature* **475**, 377–380 (2011). doi:10.1038/nature10194 Medline

45. S. Pellow, P. Chopin, S. E. File, M. Briley, Validation of open:closed arm entries in an elevated plus-maze as a measure of anxiety in the rat. *J. Neurosci. Methods* **14**, 149–167 (1985). doi:10.1016/0165-0270 (85)90031-7 Medline

46. J. N. Crawley, Neuropharmacologic specificity of a simple animal model for the behavioral actions of benzodiazepines. *Pharmacol. Biochem. Behav.* **15**, 695–699 (1981). doi:10.1016/0091-3057 (81)90007-1 Medline

47. L. K. Blumstein, J. N. Crawley, Further characterization of a simple, automated exploratory model for the anxiolytic effects of benzodiazepines. *Pharmacol. Biochem. Behav.* **18**, 37–40 (1983). doi:10.1016/0091-3057 (83)90247-2 Medline

48. R. D. E. Sewell, P. S. J. Spencer, Antinociceptive activitiy of narcotic agonist and partial agonist analgesics and other agents in the tail-immersion test in mice and rats. *Neuropharmacology* **15**, 683–688 (1976). doi:10.1016/0028-3908 (76)90037-X Medline

49. S. L. Robinson, B. A. McCool, Microstructural analysis of rat ethanol and water drinking patterns using a modified operant self-administration model. *Physiol. Behav.* **149**, 119–130 (2015). doi:10.1016/j.physbeh.2015.05.034 Medline

50. A. C. Spector, P. A. Klumpp, J. M. Kaplan, Analytical issues in the evaluation of food deprivation and sucrose concentration effects on the microstructure of licking behavior in the rat. *Behav. Neurosci.* **112**, 678–694 (1998). doi:10.1037/0735-7044.112.3.678 Medline